Research Article

Effect of spark plasma sintering temperature on the pore characteristics, porosity and compression strength of porous titanium foams

Isaac M. Makena[1] · Mxolisi B. Shongwe[1] · Ronald Machaka[2,3] · Mosimanegape S. Masete[2]

Abstract

In this work, porous titanium (Ti) foams were successfully produced using spark plasma sintering technique at four different temperatures (up to 650 °C), in conjunction with vacuum sintering (used as a post-treatment) at a constant temperature of 1200 °C. To obtain a porous structure, 60 vol% of sodium chloride was included as a pore spacer, with the addition of polyethylene glycol solution for Ti–NaCl interparticle binding. The work aimed at studying the effect of sintering temperature on the final pore features and compression resistance of the porous titanium foams. X-ray diffraction and scanning electron microscopy as characterization techniques were used to analyze phases and pore evolutions, respectively. The results showed that the pore characteristics and the final porosity of porous titanium foams profoundly depend on the sintering temperature. The lowest porosity of approximately 53.9 vol%, with denser pore walls, was seen at the highest sintering temperature. Such foams sintered at 650 °C can resist the compression stress as high as 123 MPa while exhibiting the stiffness value of 8.1 GPa. The results indicate that the porous Ti foams produced have great potential for applications in hard tissue engineering.

Keywords Spark plasma sintering · Vacuum sintering · Pore characteristics · Compression test

1 Introduction

The need for distinct properties such as resistance to corrosion, excellent biocompatibility, adequate strength, lightweight, low stiffness, etc. has enforced the choice of titanium-based materials for implant fabrications. However, concerns still subsist as the reported stiffness values of titanium materials are relatively high (≥ 45 GPa) compared to that of the human cortical bone (20–30 GPa). Such mismatches should be avoided to prevent the phenomenon of stress-shielding, which usually results in adverse effects such as bone resorption around the implant, premature revisions, etc. In addition to stiffness mismatch, most of the implants in the market are usually used as dense solid parts that most often lack the ability to attach to the host bone coherently. To counteract such implant problems, there is a broad interest in directing the research effort on developing low stiffness porous implants [1, 2].

Nevertheless, care needs to be put in place as the introduction of pores drastically reduces the strength of the material. A review on the properties of porous biomaterials such as iron-, cobalt-, and titanium-based systems by Lemons and Lucas [3] shows that depending on porosity level, the strength reduction can reach magnitudes as low as less than 50% of that of nonporous alloys. Lascano et al. [4] reported the compressive strength of sintered

dense non-porous Ti as approximately 650 MPa and that of 40 vol% porosity Ti as 150 MPa. A severe drop in compression strength of a porous NiTi material from 108.8 to 56.2 MPa, with an introduction of minor pores (i.e., total porosity increased from 53.6 to 55.1 vol%) was witnessed by Jian et al. [5]. The loss of strength with pore introduction can be related to the reduced area supporting the actual stress. That is, a decrease in the sectional area of the material reduces the pressure needed to yield. It is, therefore, the focus of this work to find the balance between strength and stiffness through manipulating fabrication variables. Xiang et al. [6] showed a strong dependence of the yield strength and Young's modulus of porous Ti on the sintering temperature, porosity, and pore size. The authors stated that an increase in sintering temperature reduces the porosity of the material and increases the resulting strength and Young's modulus. The same behavior was reported by Shao et al. [7] during an investigation of the effect of sintering temperature on the development of porous Ti–39Nb–6Zr alloy.

Several manufacturing techniques are widely used to produce porous materials. Ahmad et al. [8] used the slurry foaming method in conjunction with vacuum sintering to produce titanium foams. The use of the freeze casting technique was recently reported by Yan et al. [9]. Torres et al. [10], reports the feasibility of obtaining a porous structure by simply sintering a loose powder in a furnace, while, Szyniszewski et al. [11] and Novák et al. [12] suggest the use of hollow powder sphere and powder reactive sintering methods, respectively. The advantage of the above-mentioned techniques is that the pore features such as distribution, size, orientation, and morphology can be easily controlled. The only challenge with these conventional techniques, as spotted in the book written by James [13], is the limited porosity level, which can be achieved. One promising manufacturing route which is exploited in this study is the use of powder metallurgy in combination with the space holder technique. The use of NaCl as a space holder is widely reported for the development of porous titanium foams. NaCl is cheap, abundantly available, has high strength and high melting temperature. Ye and

Dunand [14] corroborate the use of NaCl as it possesses no health threat due to its low toxicity in the case of residual content in the implant, and for that, it is considered a suitable spacer material. However, the melting point at which NaCl starts to soften and melts is relatively low for titanium particles to bind with adequate strength. Such drawbacks can be offset by the use of spark plasma sintering (SPS), which brings with it the ability to sinter the powder at relatively lower temperatures compared to other conventional powder metallurgy sintering techniques. The SPS is a fast, environmentally sustainable powder sintering technology which integrates plasma activation, hot pressing, and resistance heating, and directly connects the high-frequency pulse current between the pressurized powder particles. Complementarily, vacuum sintering will be used to post-treat the specimen after the space holder removal to increase the strength of the foams. Vacuum space will help in limiting the titanium specimen contamination and oxidations.

This study precisely aims to examine the effect of SPS temperature on the final pore characteristics and compression resistance of the porous titanium foams. The foams are developed using a two-step sintering: spark plasma sintering—vacuum sintering, with NaCl particles used as space holders.

2 Experimental procedure

2.1 Powders preparation and consolidation

Commercially pure titanium powder of Grade 1, supplied by TLS Technik GMBH & Co. (Germany), having an average size of ≤ 25 μm particle size was blended with NaCl granules (99% purity, 212 μm ≥ particle size ≤ 425 μm). To avoid the occurrence of Ti–NaCl particle separation through segregation, a liquid polyethylene glycol (PEG-400) amounting to approximately 1 wt% of the mixture was added as a binder. The morphological characteristics of the powders used are shown in Fig. 1a, b. The powder particles of Ti have a smooth

Fig. 1 SEM micrograph of titanium (**a**) and sodium chloride powders (**b**)
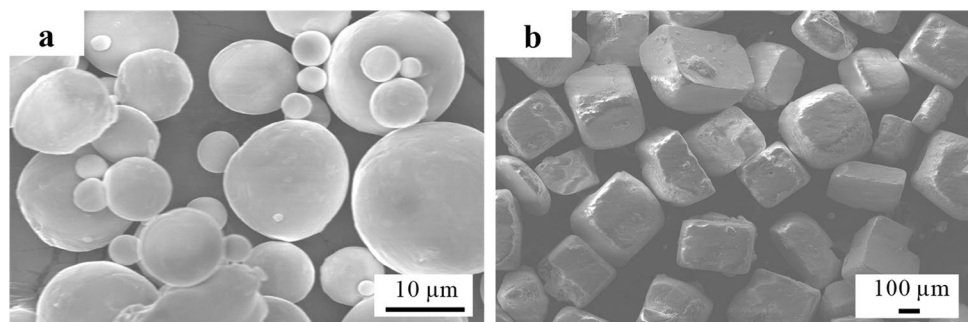
spherical surface, while NaCl granules are cubic-cuboidal in shape with round angles. A schematic diagram summarizing the flow of the whole fabricating process is shown in Fig. 2, with steps 1–3. As written in the process flow, fabrication consisted of three stages, i.e., spark plasma sintering (HPD5, FCT SPS Systeme GmbH, and Germany) at 500 °C, 550 °C, 600 °C, or 650 °C, desalting and post-treatment at 1200 °C for 60 min.

Figure 2—*Step 1*; Sintering was conducted at either of the four different temperatures to produce compacts of 20 mm diameter and 8 mm in height. The varying of temperatures is within the effort to obtain an optimum temperature, which gives the highest strength without softening or melting the salt. During sintering, the pressure and heating rate of 50 MPa and 50 °C/min, respectively, were kept constant throughout the cycle. As shown on the profile, the only parameter which was varied in this work was SPS temperature; and is thus often referred to as sintering temperature. Samples were allowed to cool inside the sintering chamber, which uses a water-cooling coil system. *Step 2*; The NaCl space-holder dissolution method followed by ultrasonic cleaning treatment was used. For more information on the fabrication details, the reader is referred to the work of Makena et al. [15].

It should be noted that up to this stage, the foams produced do not possess adequate strength for handling, consequently resulting in the need for further treatment. *Step 3*; **v**acuum (10^{-4} mbar) sintering was then employed as a post-treatment to strengthen the foams. A constant heating rate of 10 °C/min is applied throughout the cycle, after which the furnace is switched off to allow the samples to cool inside.

2.2 Materials characterization

Sample preparations upon removal from the post-treatment furnace involved wire cutting (CUT20, Agie-Charmilles) into chunks of appropriate dimensions required for characterizations and compression tests, i.e., length of 7.30 mm, the width of 7.30 mm and height of 12 mm. The analysis of pore morphological features and phases of samples was done by scanning electron microscopy (SEM, Carl-Zeiss) and X-ray diffraction (XRD, Cu-Kα radiation, PANalytical Empyrean model), respectively. The apparent density of the foams was measured and compared to the theoretical density of the solid titanium to estimate the porosity of the foams (Makena et al. [15]). Instron 1342 servo-hydraulic testing machine with a load cell capacity of 25 kN was used to determine the compression strength. The compression machine speed was set at 0.5 mm/min and stopped after the compression strain of 20%.

3 Results and discussion

3.1 Phase analysis

The XRD results of the sintered porous titanium specimens are presented in Fig. 3. The XRD pattern of pure Ti powder was also included for comparison purposes. A typical close-packed hexagonal (α-hcp) lattice of Ti is detected as the main phase for all the samples, and the diffraction peaks are similar in shape. However, the intensity of the sintered foam peaks is extremely low compared to that of the powder, and this can be attributed to the sample surface morphology effect, as was also observed by Jamaludin et al. [16]. As the temperature
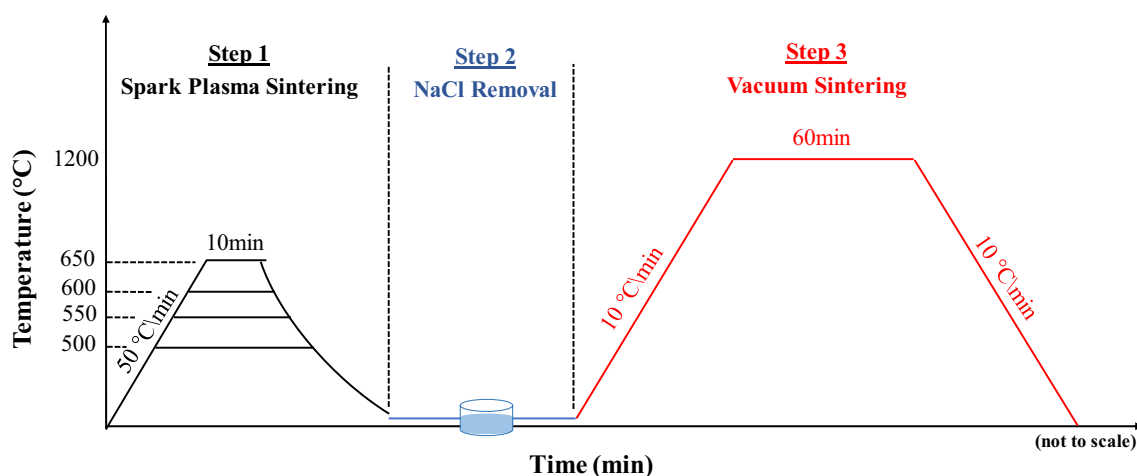

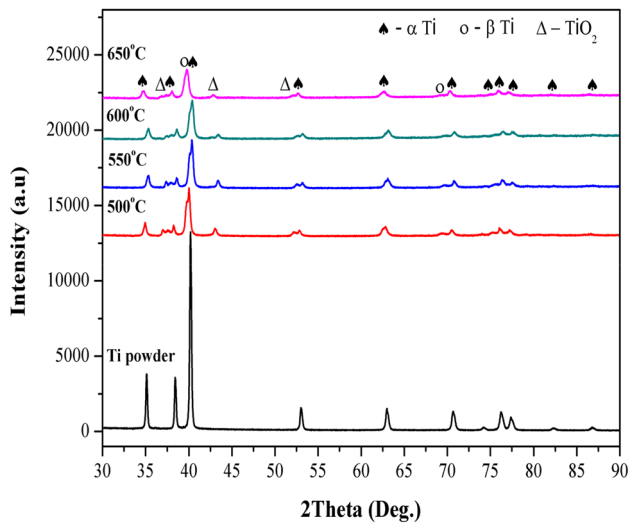**Fig. 2** Process route to fabricate porous Ti foams

Fig. 3 XRD patterns of raw Ti powder and foams sintered at varying temperatures: 500, 550, 600, and 650 °C

increases, there is a slight shift of the Ti peak at an angle of $2\theta = 40.195°$ $(10\bar{1}1)$ to lower angles. This might be due to the fading away of the α-peak in expense to the formation of β-phase, which is ambiguously seen on the patterns. The figure also shows the presence of Ti oxide (TiO_2) in the sintered samples, and it is observed that the

oxide characteristic peaks shorten with an increase in temperature. The presence of this oxide is formed either from the reaction of the Ti surface with the decomposing gases from the PEG-400 binder ($C_{2n}H_{4n+2}O_{n+1}$) or with the residual air trapped in the sample. The shortening of the TiO_2 peak with temperature can be linked to the benefits acquired when using SPS. As reviewed by Matizamhuka [17], the SPS technique can produce sparks on the powder surface, which then breaks and remove the oxide layer. Nonetheless, no detrimental impurities such as Cl, NaCl, $TiCl_4$, etc. could be detected in the sintered porous Ti structures.

3.2 Pore characteristics

The SEM micrographs depicting the effect of sintering temperature on porous Ti pore features are shown in Figs. 4 and 5. From Fig. 4a, c, we can see that the rectangular shapes of the solid NaCl particles are well replicated and that the foams structures are firm for soft handling after desalting. Looking at Fig. 4b, d, the rectangular shapes and connectivity holes of the macropores are still distinct even after conducting the post-treatment at a markedly high temperature. The average diameter size of the pores is maintained above 100 μm as required; Jian et al. [5] recommend an average pore size larger than 100 μm to allow
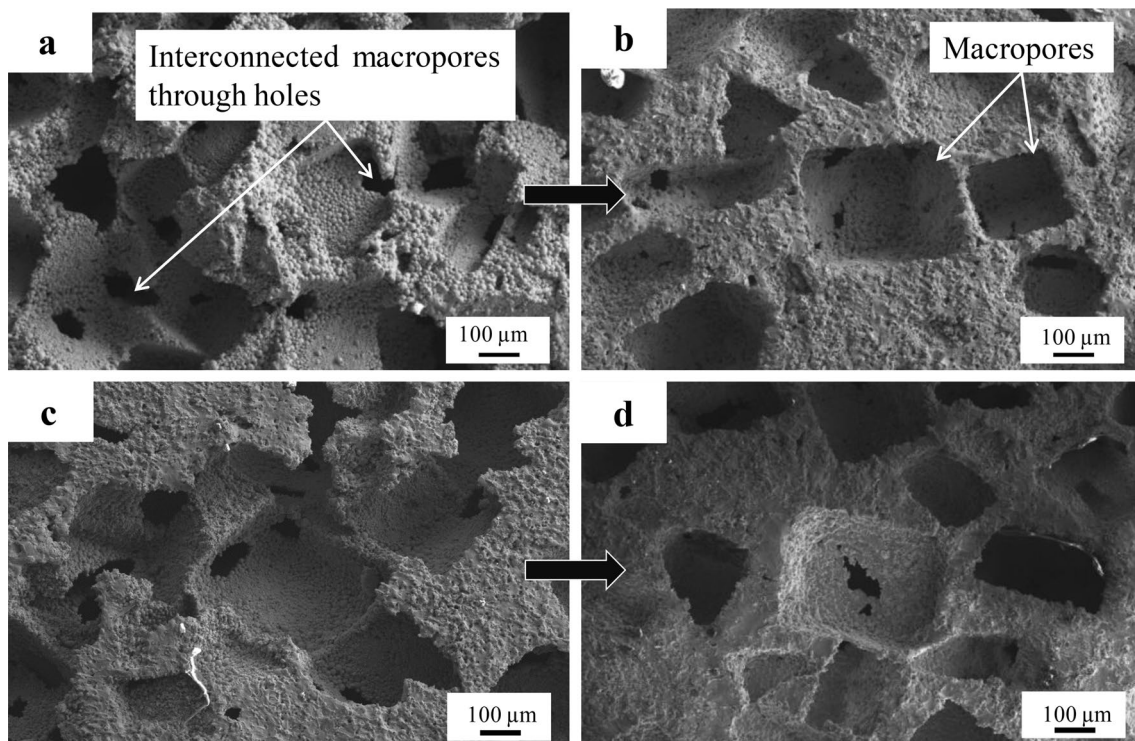

Fig. 4 SEM surface micrographs of as-sintered specimen, **a** 500 °C, **c** 650 °C, and post-heat treated **b** 500 °C + 1200 °C, **d** 650 °C + 1200 °C porous Ti foams
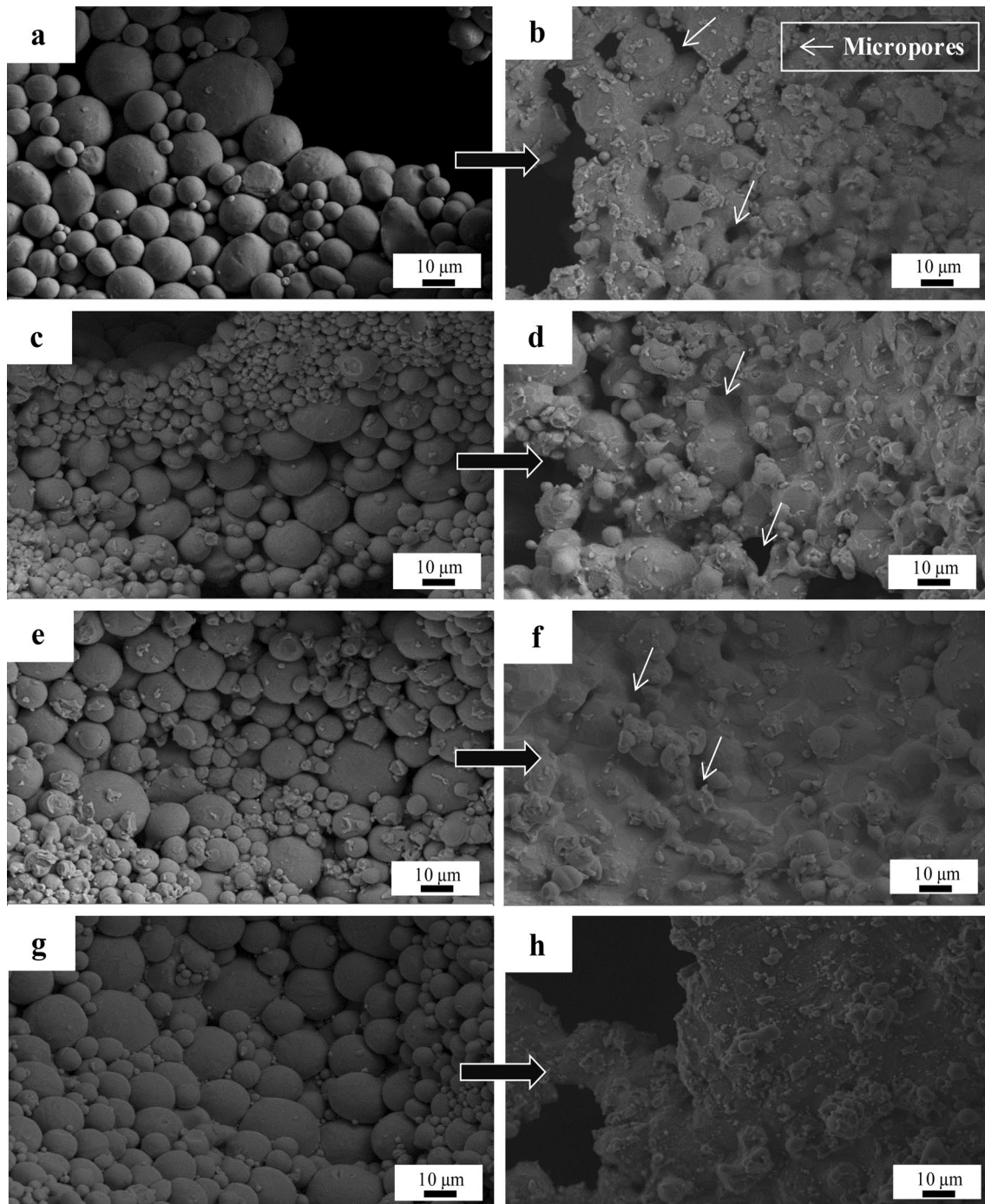
Fig. 5 SEM micrographs of foams macropore walls sintered at different temperatures, **a** 500, **c** 550, **e** 600, **g** 650 °C, and sintered plus heat-treated (**b**, **d**, **f**, **h**)

for bone tissue ingrowth. From Fig. 5a, c, e, g, original Ti powder particles are seen on the pore walls, and it is only after an introduction of the post-treatment step that these particles merge to form a dense solid wall (Fig. 5b, d, f, h). The samples sintered at a higher temperature of 600 °C or above shows relatively low wall microporosity (see white arrows) and surface roughness; the micropores are seen

to be progressively closing with temperature. To clearly understand this phenomenon, we consulted with the work of Makena et al. [15]. We observed that there is a significant increase in the quantity (necking sites) and intensity (neck size) of necking during spark plasma sintering with temperature. Furthermore, a schematic illustration in Fig. 6 was included to describe the contribution of both grain
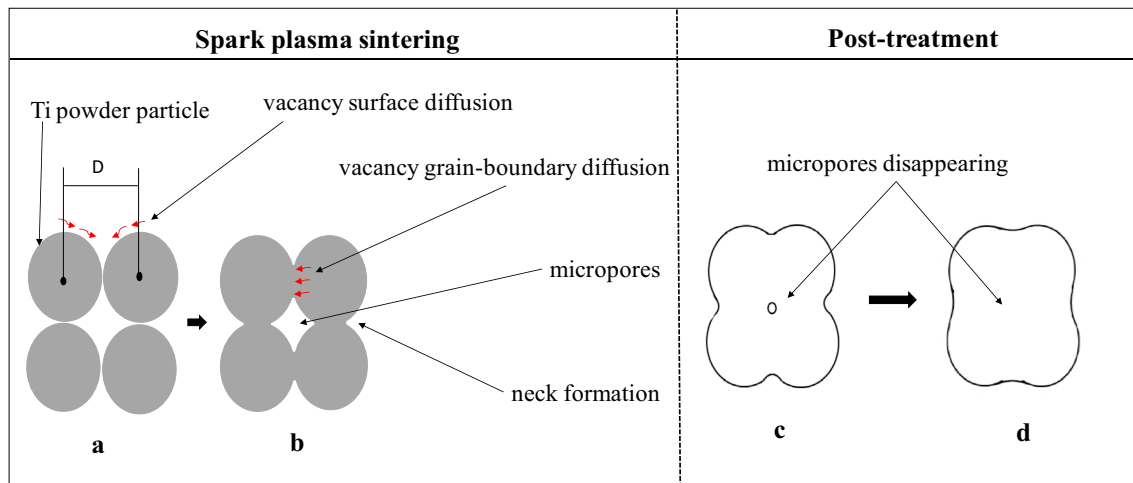
Fig. 6 Schematic diagram of the four-particle sintering model in two dimensions (a–d); D represents the distance between particles, while the short red arrows are for a mass movement of atoms

boundary and surface diffusion on pore wall densification during sintering. Mass movement takes place along the free surfaces (Fig. 6a) and grain boundaries (Fig. 6b) of particles. The model, as was reported in the work of Wakai and Brakke [18], suggests the grain boundary and the surface near the neck as the perfect sinks of vacancies for diffusions which results in particle motion during mass transportations. Therefore, we can conclude that the samples sintered at higher temperatures had facilitated atoms movement during sintering, which then consequently augmented wall densifications. Figure 6c, d depicts the effect of post-treatment on the wall densification, and it is at this stage that most of the wall microspores disappear.

3.3 Porosity measurements and compression tests

Figure 7 evaluates the effect of changing the sintering temperature on the foam's total porosity. Porosity values reported here before vacuum sintering, that is before post-treatment, were taken elsewhere from the work of Makena et al. [15]. The measured porosity corresponds very well with the design value of 60 vol%, and decreases with increasing sintering temperature. Such observations can be linked with the proposed facilitated mass movement, which takes place at higher temperatures. Furthermore, a drastic reduction of porosity is observed after post treating the samples, and it is worth to note that the degree of reduction is becoming dominant as the temperature increase. This can be attributed to the high number of already-established sintering necks that are obtained at higher sintering temperatures.

The stress–strain curves, enlarged elastic region, compression strength, and bulk elastic modulus of porous Ti foams sintered at four different temperatures are shown
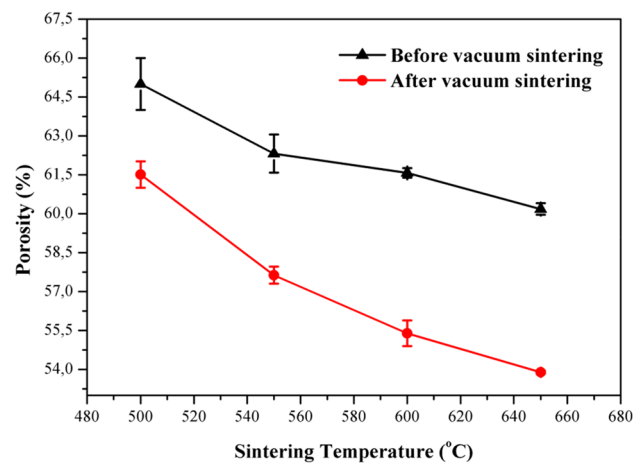

Fig. 7 Porosity of sintered porous titanium as a function of sintering temperature

in Fig. 8. As seen in Fig. 8a, the foams exhibit similar stress–strain behavior. The curves of the foams consist of two distinct regions: (1) an elastic deformation region, where the relation between stress and strain is approximately linear; this is the stage where macropore walls and edges of the porous material are believed to be only bending, and if the stress is applied and released along this line, the material will expand back to the original shape without deformation, and (2) plastic (plateau) deformation region, where the stress increases slowly or even remains constant with the strain increasing. In this plateau phase, the pressure applied is adequate to break the contact between the pore wall Ti particles, which eventually results in the collapse of the entire matrix. However, the progression of these curves appears to be incomplete in accordance with the theory of Gibson–Ashby [19]. The theory suggests
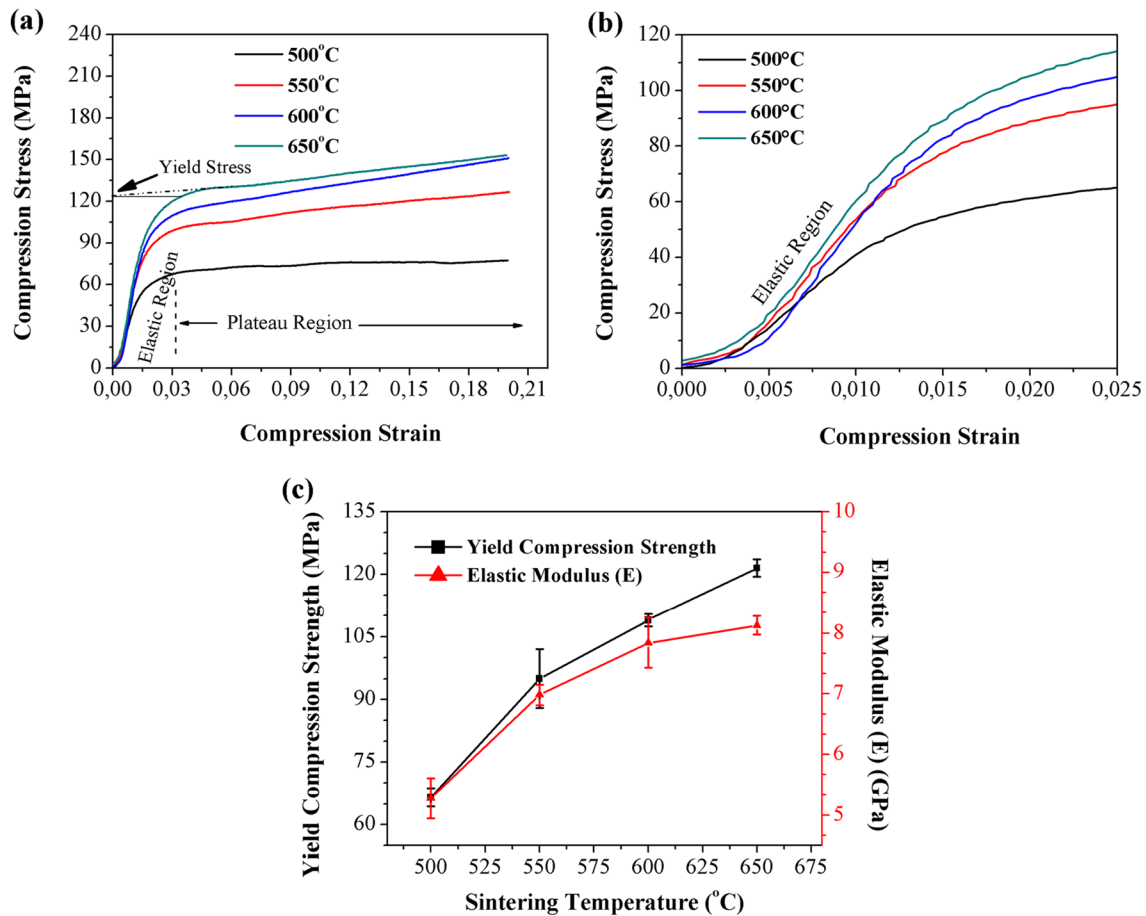
Fig. 8 Compression stress–strain curves (**a**), enlarged elastic region (**b**), and compression strength and elastic modulus (**c**) of porous Ti sintered at different temperatures: 500, 550, 600 and 650 °C

three distinct stages, i.e., elastic stage, plastic stage, and densification region, under compression loading. The densification stage does not appear in this study. It can be due to the premature release of the compression force at the strain of 20%, which was done to avoid an undesirable collapse of the foams sintered at lower temperatures.

The compression strength (yield stress) of the materials was defined by extrapolating the plateau region to strain = 0, as shown in Fig. 8a. The linear part (elastic region) of the curves was explored to estimate the Elastic modulus values of the foams. The zoomed Elastic behavior of the samples sintered at different temperatures is shown in Fig. 8b, and visually supports the Elastic modulus values reported in Fig. 8c. An increase in sintering temperature increases the foam's compression resistance from ~ 65 to 123 MPa and stiffness from ~ 5.3 to 8.1 GPa. These increments were expected as the pore walls get well densified, with an improved bonding strength within metal powder particles when the temperature increase. For samples sintered at lower temperatures, i.e., 500 and 550 °C, the sintering process is inadequate, resulting in higher total porosity

and reduced compressive strength. It should be noted that the strength and stiffness values obtained in this study are comparable to that of the human bone (~ 130 MPa, and elastic modulus of ≤ 30 GPa), and can be regarded as potential future tissue replacement materials.

4 Conclusions

Porous Ti foams were successfully fabricated using a two-step sintering method: spark plasma sintering—post-treatment, with NaCl particles used as space holders. The effects of the SPS temperature on the pore characteristics, porosity, and compression strength were studied.

1. Pore walls become denser with no significant changes in the overall pore shape as the sintering temperature is increased.
2. The final porosity level of the foam profoundly depends on the sintering temperature. Titanium foams with porosities diminishing from 61 to 54 vol% were

obtained with an increase in temperature. The porosity of the foams is further reduced during post-treatment, which closes micropores, and the degree of reduction becomes more dominant at higher sintering temperatures.

3. The highest compressive strength of 123 MPa was obtained at a temperature of 650 °C. Stiffness values reported in this work with an increase in temperature were extremely low, i.e., 5.3–8.1 GPa. Such values suggest that these porous Ti foams can withstand relatively heavy loads with less stress shielding effect and thus, can be considered as promising biomedical materials.

Compliance with ethical standards

Conflict of interest The authors declare that they have no conflict of interest.

References

1. Li Y, Yang C, Zhao H, Qu S, Li X, Li Y (2014) New developments of Ti-based alloys for biomedical applications. Materials 7:1709–1800
2. Aherwar A, Singh A, Patnaik A (2016) Current and future biocompatibility aspects of biomaterials for hip prosthesis. AIMS Bioeng 3:23–43
3. Lemons JE, Lucas LC (1986) Properties of biomaterials. J Arthroplasty 1:143–147
4. Lascano S, Arévalo C, Montealegre-Melendez I, Muñoz S, Rodriguez-Ortiz JA, Trueba P, Torres Y (2019) Porous titanium for biomedical applications: evaluation of the conventional powder metallurgy frontier and space-holder technique. Appl Sci 9:1–13
5. Jian YT, Yang Y, Tian T, Stanford C, Zhang XP, Zhao K (2015) Effect of pore size and porosity on the biomechanical properties and cytocompatibility of porous NiTi alloys. PLoS ONE 10(6):e0128138
6. Xiang C, Zhang Y, Li Z, Zhang H, Huang Y, Tang H (2012) Preparation and compression behavior of porous titanium prepared by space-holder sintering process. Proc Eng 27:768–774
7. Shao Y, Song X, Ye W, Hui S, Yu Y, Liu R, Li C (2016) Effect of sintering temperature on porous structures and mechanical properties of Ti–39Nb–6Zr alloys. Mater Sci Forum 848:532–537
8. Ahmad S, Muhamad N, Muchtar A, Sahari J, Ibrahim MHI, Jamaludin KR, Nor NHM, Murtadhahadi I (2010) Development and characterization of titanium alloy foams. Int J Mech Mater Eng 5:244–250
9. Yan L, Wu J, Zhang L, Liu X, Zhou K, Su B (2017) Pore structures and mechanical properties of porous titanium scaffolds by bidirectional freeze casting. Mater Sci Eng C 75:335–340
10. Torres Y, Pavón JJ, Rodríguez JA (2012) Processing and characterization of porous titanium for implants by using NaCl as a space holder. J Mater Process Technol 212:1061–1069
11. Szyniszewski ST, Smith BH, Hajjar JF, Schafer BW, Arwade SR (2014) The mechanical properties and modeling of a sintered hollow sphere steel foam. Mater Des 54:1083–1094
12. Novák P, Salvetr P, Školáková A, Karlík M, Kopeček J (2017) Effect of alloying elements on the reactive sintering behavior of NiTi alloy. Mater Sci Forum 891:447–451
13. James WB (2015) Powder metallurgy methods and applications. In: Samal P, Newkirk J (eds) Powder metallurgy, ASM handbook, vol 7, pp 9–19
14. Ye B, Dunand DC (2010) Titanium foams produced by solid-state replication of NaCl powders. Mater Sci Eng A 528:691–697
15. Makena IM, Shongwe MB, Machaka R, Matizamhuka WR (2019) Influence of spark plasma sintering temperature on porous titanium microstructural integrity, airflow resistance, and space holder removal. Int J Adv Manuf Technol 104:2501–2511
16. Jamaludin MI, Kasim NAA, Nor NHM, Ismail MH (2015) Development of porous Ti_6Al_4V mix with palm stearin binder by a metal injection molding technique. Am J Appl Sci 12:742–751
17. Matizamhuka WR (2016) Spark plasma sintering (SPS)—an advanced sintering technique for structural nanocomposite materials. J South Afr Inst Min Metall 116:1171–1180
18. Wakai F, Brakke KA (2011) Mechanics of sintering for coupled grain boundary and surface diffusion. Acta Mater 59:5379–5387
19. Gibson LJ, Ashby MF (1997) Cellular solids: structure and properties, 2nd edn. Cambridge University Press, New York, pp 195–207